Supporting Information for

Strong HONO Emissions from Fertilized Soil in the North China Plain Driven by Nitrification and Water Evaporation

Chaoyang Xue[1, 2, *], Can Ye[1, 4], Pengfei Liu[1], Chenglong Zhang[1], Hang Su[3], Fengxia Bao[3], Yafang Cheng[3], Valéry Catoire[2], Zhuobiao Ma[1], Xiaoxi Zhao[1], Keding Lu[4], Yuhan Liu[4], Max R. McGillen[5], Abdelwahid Mellouki[5], Yujing Mu[1, *]

[1] Research Centre for Eco-Environmental Sciences, Chinese Academy of Sciences, Beijing 100085, China

[2] Laboratoire de Physique et Chimie de l'Environnement et de l'Espace (LPC2E), CNRS–Université Orléans–CNES, Cedex 2, Orléans 45071, France

[3] Max Planck Institute for Chemistry, Mainz 55128, Germany

[4] State Key Joint Laboratory of Environment Simulation and Pollution Control, College of Environmental Sciences and Engineering, Peking University, Beijing, 100871, China

[5] Institut de Combustion Aérothermique, Réactivité et Environnement, Centre National de la Recherche Scientifique (ICARE-CNRS), Cedex 2, Orléans 45071, France

Correspondence:

Chaoyang Xue (chaoyang.xue@cnrs-orleans.fr)

Yujing Mu (yjmu@rcees.ac.cn)

Content

1 Field Campaign

1.1 Fertilizer Application around the SRE-CAS Station

According to the cultivation habit of the local farmers, synthetic fertilizer (e.g., $N(NH_4Cl)$: P_2O_5: K_2O=22%: 8%: 15%) was popularly used for summer maize planting. The fertilizer application rate in the NCP carried from 120 to 729 kg-N ha^{-1}, and about 200-330 kg-N ha^{-1} was typically used for the fields of nearby villages around the SRE-CAS station. Even higher fertilizer application rates (e.g., 3000 kg-N ha^{-1} y^{-1}) were used for vegetable cultivation in the NCP[1].

1.3 Field Measurements of Soil HONO Emission Fluxes

Six sets of flux measurements were conducted at the SRE-CAS station, including twice in summer 2015, three times in summer 2016, and once in summer 2017 (Table S2). In the summer of 2015, the main task was to test the performance of the OTC system. The interference in HONO emission flux measurement and the interruption of the soil environment were both found to be small. Peak HONO emission flux before fertilization (treated as a fertilizer application rate of 0 kg-N ha^{-1}) was about 3 ng-N m^{-2} s^{-1}. This is in agreement with recent flux measurements over agricultural or grass fields[2,3]. After fertilization with 45 kg-N ha^{-1}, peak emissions increased to 40 ng-N m^{-2} s^{-1}, which was driven by soil emissions (see the main text).

Since about 200-330 kg-N ha^{-1} was typically used for the fields of nearby villages around our station, in the summer of 2016, we repeated flux measurements from 27 June to 15 July 2016 with a fertilizer application rate of 330 kg-N ha^{-1}. Unfortunately, the measurement was frequently interrupted by strong rain events, but we still observed a maximum emission flux of 1515 ng-N m^{-2} s^{-1}. The data from the two campaigns were presented in Xue et al. (2019)[4].

To explore the integral variation of HONO emission flux after fertilization, we repeated the measurements from 19 August to 6 September 2016 with a fertilizer application rate of 247 kg-N ha^{-1}, of which the corresponding data was demonstrated in Figure 1 in the main text. Two days of flux measurement before fertilization was also conducted.

In summer 2017, we reduced the fertilizer application rate to 180 kg-N ha^{-1}. Based on all our six sets of flux measurements, the emission characteristics of soil HONO emissions could be studied. In addition, it also provides insights into the relationship between HONO emission fluxes and the fertilization application rate (Table S2 and Figure S6).

1.5 Measurements of Atmospheric Pollutants

During the field campaigns, the concentrations of atmospheric NO_x (NO, NO_2) and NO_y

(the sum of the reactive nitrogen oxides, including NO, NO_2, PAN, HNO_3, HONO, particulate nitrate, etc.) were measured by Model 42i-NO_x analyzer (Thermo Scientific, USA) and Model 42i-NO_y analyzer (Thermo Scientific, USA), respectively. H_2O_2 was measured by a commercial instrument (AL2021 AEROlaser, Germany). $PM_{2.5}$ was measured by a standard tapered element oscillating microbalance system (TEOM 1400A, Thermo Scientific, USA). See Table S1 for detailed information on instruments involved in our campaigns.

1.6 Measurements of Meteorological Parameters

The total solar radiation, ambient temperature, relative humidity (RH), wind speed, wind direction, and soil temperature (depth: 5 cm) were automatically measured and recorded by an auto meteorological station at the SRE-CAS station.

1.7 Measurements of Soil Parameters

During the HONO flux measurement period, soil parameters were also measured synchronously. Three soil samples were collected every two days to measure the concentrations of soil water content (% WHC), soil nitrite, soil nitrate, and soil pH. Each soil sample was divided into three parts: one for measuring the SWC by quantifying the soil weight before and after heating in an oven at 105 °C for 24 hours, one for measuring the soil pH based on the method of ISO 10390:2005-2012, and the other for measuring the soil nitrite and nitrate concentration based on the method of ISO/TS 14256-1:2003 (E).

For comparison with the values of soil water content (SWC) reported by previous studies, the SWC in this study was calculated based on the water-holding capacities (WHC), which is derived from the equation:

$$WHC = \frac{m_{sat-water}}{m_{dry-soil}} \quad (3)$$

where $m_{sat\text{-}water}$ is the weight of soil water under the condition of the soil saturated with water and $m_{dry\text{-}soil}$ is the mass of the soil after heating at 105 °C for 24 hours. The SWC in % WHC is the proportion of the weight of soil water to $m_{sat\text{-}water}$.

2 Laboratory Simulation Experiments

2.1 Collection of Soil Samples

The surface soil at an approximate depth of 5 cm in the agricultural field was collected by a scoop into a knitted bag. Soil samples were then sieved by a 2-mm sieve and stored in a refrigerator at 4 °C. The initial SWC of soil samples was measured by quantifying the soil weight before and after heating in the oven at 105 °C for 24 hours.

For each experiment, ca. 75 g soil sample was filled into a glass tank with a surface area of 0.08 m^2, humidified to 90% WHC by the water solutions of various fertilizers, and then incubated at a growth chamber (temperature: 20 °C; relative humidity: 80%; dark condition).

2.2 Treatments on Soil Samples

2.2.1 Influence of Soil Temperature, Soil Bacteria, and Fertilizer Types

Well-mixed soil samples were divided into three parts (defined as S1, S2, and S3). S1 was sterilized by an autoclave at a given pressure (0.1 MPa) and temperature (121 °C) for 1 hour. This could kill the microbes in the soil but didn't change other properties of the soil. Then, S1, S2, and S3 were fertilized by NH_4Cl, NH_4Cl, and KNO_3 solutions, respectively, with a constant fertilizer application rate of 400 mg-N kg^{-1} soil. This fertilizer application rate is equal to ~250 kg-N ha^{-1} for field conditions. To keep the variation of soil water content similar to field conditions, i.e., small changes in soil water contents within one week after fertilization (80-90%WHC), soil samples were initially wetted to 90%WHC and the water loss was replenished through spraying water on the soil surface after daily measurements.
During each incubation day, HONO and NO emissions were measured for 1 h at 18 °C followed by 1 h at 35 °C. Soil temperature was controlled by circulating water from two thermostat water baths. RH of the flushing gas was 61.7%. Results are shown in Figure 2 in the main text.

2.2.2 Influence of RH and Soil Water Evaporation

Three NH_4Cl-treated (400 mg-N kg^{-1}) soil samples were used to explore the impacts of the RH of the carrier gas. For each sample, HONO emission was measured for 1 h. The RH of the carrier gas was set at 48.8% for the first 30 min measurement. After that, it was set at 0% (dry synthesis air) for another 30 min. Results are shown in Figure 3A.
To quantify the impact of soil water evaporation, HONO emission from NH_4Cl-treated soil samples was measured under gradient RH levels. During each RH step, soil water loss (Δm) was recorded by the difference in the total soil weight before and after each experiment. Weight loss caused by gas emissions other than water evaporation has negligible impacts on Δm as they are several orders of magnitude lower than water loss. The average water evaporation rate (E_{water} in g min^{-1}) could also be obtained according to Δm and experimental time. During those experiments, HONO emissions at each RH step were measured for 30 min at 35 °C. Results are shown in Figures 3B and 3C.

2.2.3 Influence of Nitrification inhibitors

Well-mixed soil samples were divided into three parts (defined as S4, S5, and S6). All the samples were treated with 100 mg-N (NH_4Cl) kg^{-1} soil and wetted to 90% WHC. S5 and S6 were additionally treated with 5 and 10 mg-DCD kg^{-1}, respectively. HONO and NO emissions from those three samples were measured every day for 30 min. The

soil temperature was controlled at 25 °C, and dry air was used in the experiment to accelerate HONO release from soil samples, to assess the performance of DCD.

3 Model Simulations

It is well known that the implementation of HONO chemistry in models, including box models[5–7], regional chemistry-transport models[8–13], and global models[14,15], could enhance the atmospheric oxidizing capacity (AOC) and the formation of secondary pollutants like aerosols and O_3. Moreover, several studies also pointed out that soil HONO emissions could have significant impacts on regional AOC and O_3 levels[6,13,16]. However, all those simulations are constrained by estimated HONO emission flux. With constraint by field flux measurements, similar enhancements in AOC and O_3 should be expected, but with more quantitative discussion and conclusion.

To explore the regional impacts, such as the enhancements in AOC and O_3, soil HONO emissions were implemented into the RACM v2 model (Regional Atmospheric Chemistry Mechanism v2, box model).

However, due to the limitation of available field data, model simulations could not be run for the summer of 2016. Instead, we ran box model simulations for the summer of 2014 when a comprehensive field campaign (including measurements of VOCs, radicals, O_3, NO_x, J-values, etc.) was conducted at a site near our station (about 2 km)[6]. Because similar fertilizer types and application rates were used in this region every summer for planting summer maize, similar HONO emission variations were also expected each year after planting summer maize. This could be also confirmed by our several field flux measurements in the summers of 2015-2017. Therefore, we used the HONO emission flux obtained in the summer of 2016 for model simulations.

Due to the above facts, model simulations of regional impacts may suffer uncertainties, but the quantifications are more representative for this region considering that this is the first time to include the first field flux measurements in the models. Details about the model description will be presented in the following sections.

3.1 RACM2 Simulations

A 0-D box model RACM2 was adopted to explore the influence of HONO emission from the fertilized soil on atmospheric HONO levels as well as O_3 formation rates. The mechanism in the model contains 17 stable inorganic compounds, 4 inorganic intermediates, 55 stable organic compounds, and 43 organic intermediates[17].

The model was constrained by the field observation data in the summer of 2014 at the approximately same sampling site as this study (the distance between the two sampling sites is about 2 km)[6]. Note that the campaign in the summer of 2014 covered one period of fertilization. As Liu et al.[6] suggested, high levels of observed HONO could not be explained by reported sources. Since the period (from 8 June to 5 July) of this campaign in 2014 also covered the intensive fertilization event for the summer maize planting,

significant HONO emissions from fertilized agricultural fields are inferred to explain the observations during this campaign. This also indicates the common presence of soil HONO emissions after regular fertilization every year.

Details about the model settings and constraints could be found in Liu et al.[6] In this study, we implemented the averaged diurnal HONO emission flux in the RCAM2 model. Two model scenarios were set: one default mechanism that only contained the homogeneous HONO formation (without flux), and the other one with soil HONO emissions as input (with flux).

As shown in Figure S8, the simulated and measured HONO concentrations were in good agreement when soil HONO emission was considered, whereas the HONO concentrations simulated without soil HONO emissions were one magnitude less than the observations. Additionally, O_3 production rates during daytime increased by more than 50% after consideration of soil HONO emissions.

4 Tables

Table S1: Instruments used in the field campaigns.

Analyzer	Parameter	Detection limit	Measurement principle	Resolution
Thermo Scientific Model 42i-Y, USA	NO/NO_y	0.5 ppbv	Chemiluminescence	1 min
Thermo Scientific Model 42i, USA	NO/ NO_x	0.4 ppbv	Chemiluminescence	1 min
SC-IC	HONO	20 pptv	Ion chromatography	1 hour
LOPAP-03, QUMA, Germany	HONO	5 pptv	Long path liquid absorption	1 min
Thermo Scientific Model 49i, USA	O_3	0.5 ppbv	UV absorption	1 min
Thermo Scientific 1405 TEOM, USA	$PM_{2.5}$	2 $\mu g\ m^{-3}$	Tapered element oscillating microbalance	1 min
AL2021 H_2O_2 analyzer, AEROlaser, Germany	H_2O_2	0.1 ppbv	liquid chemistry fluorescence	1 min
Thermo Scientific Model 43i, USA	SO_2	0.5 ppbv	Pulsed fluorescence	1 min
Seal Analytical AutoAnalyzer 3, USA	Soil NO_3^-	0.1 $\mu g\ L^{-1}$		1 day
Mettler Toledo Delta 320 pH Analyzer, USA	soil pH	0.1		1 day

Table S2: Maximum F_{HONO} and fertilizer application rates.

Measurement Period	Fertilization Rate (kg-N ha^{-1})	F_{HONO}_max (ng-N m^{-2} s^{-1})	F_{HONO}_average (ng-N m^{-2} s^{-1})
10-14 Aug. 2015	0	3.2	1.9±0.9
10-14 Aug. 2015	45	40.4	21.0±11.3
27 Jun.-24 Jul. 2016	330	1515	187±261
11-12 Aug. 2016	0	4.6	3.5±0.7
19 Aug.-6 Sept. 2016	247*	348	34.5±53.2
13-21 Jun. 2017	180	161	19.9±26.9

*: the typical fertilizer application rate by local farmers

5 Figures

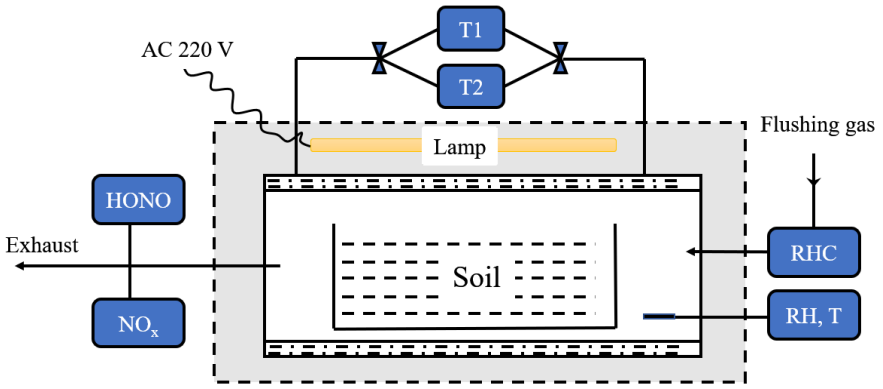

Figure S1. Diagram of the flow tube. T1 and T2 represent the two thermostatic water baths; RHC represents the relative humidity controller system.

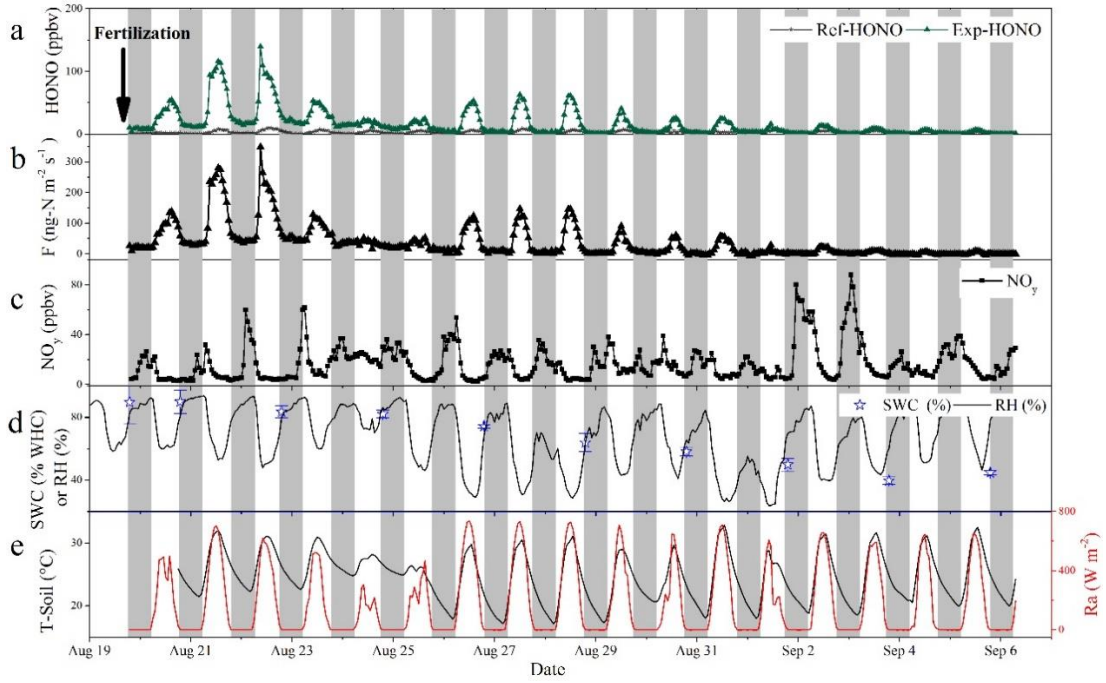

Figure S2. Time series of the measured HONO emission flux and related parameters. a: HONO concentrations in the experimental chamber (Exp-HONO) and reference chamber (Ref-HONO). Note that information about ambient HONO was presented in Figure S3; b: Soil HONO emission fluxes (F_{HONO}); c: ambient concentrations of total reactive nitrogen (NO_y); d: soil water content (SWC in %WHC) and atmospheric relative humidity (RH); e: soil temperature (T-Soil) and solar irradiance (Ra). The down arrow shows the date of fertilization (247 kg-N ha^{-1}, typical compound fertilizer used by local farmers, N: P_2O_5: K_2O=24: 12: 6), and the shallowed regions represent nighttime periods.

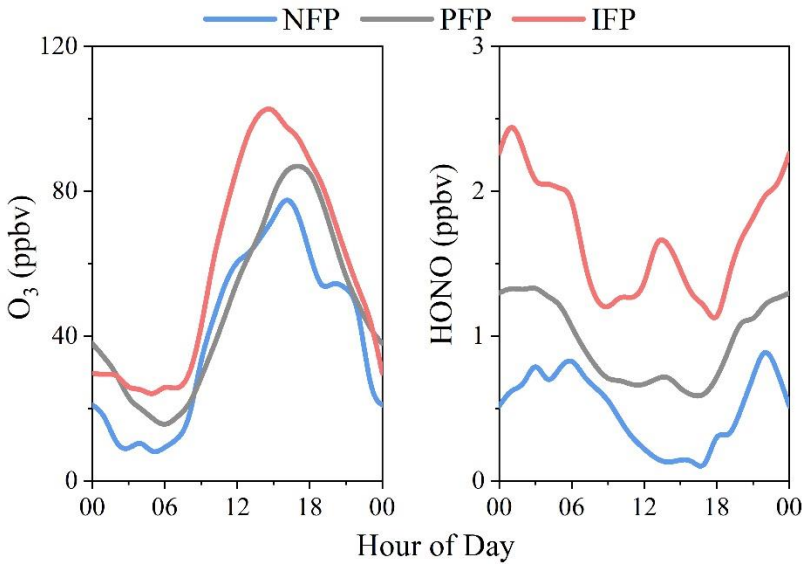

Figure S3. Average diurnal profiles of HONO and O_3 measured at the SRE-CAS site in the summer of 2017[18]. NFP: before fertilization period; PFP: pre-intensive fertilization; IFP: intensive fertilization period.

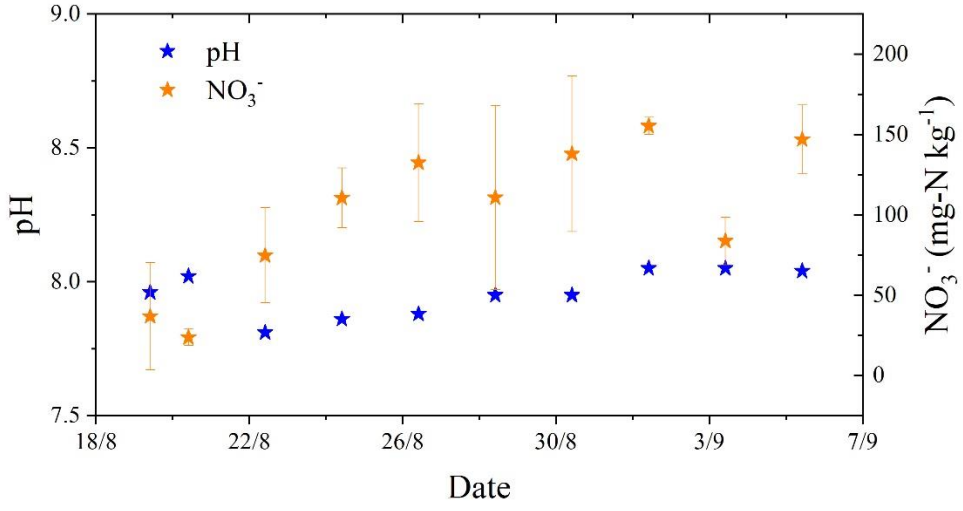

Figure S4: The measured soil pH and NO_3^- concentration during the campaign from 19 Aug. to 6 Sept. 2016. Error bars for NO_3^- curve represent the standard deviation of three soil samples.

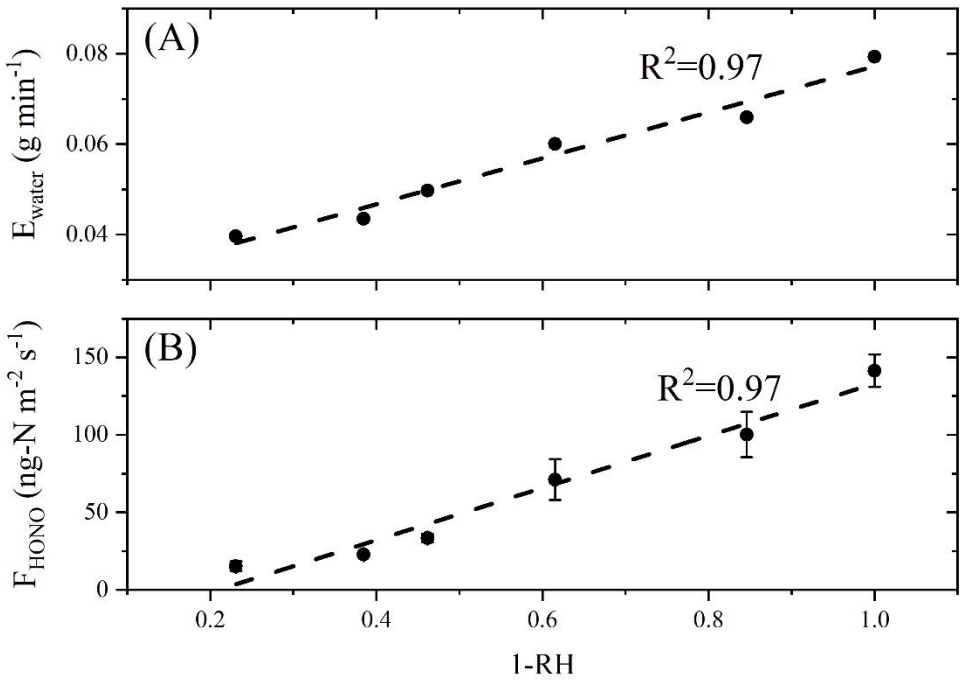

Figure S5: (A) The correlation between soil water loss rate (E_{water}) and 1-RH and (B) the correlation between the HONO emission flux (F_{HONO}) and 1-RH during the gradient RH experiment.

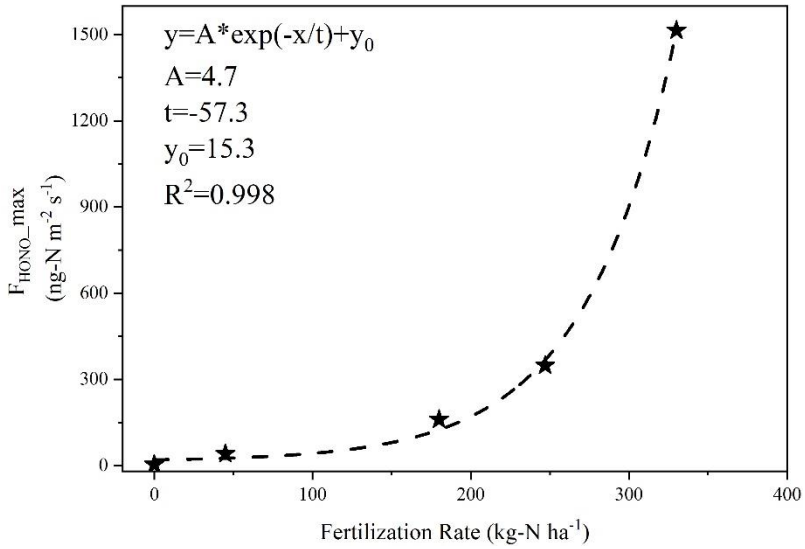

Figure S6: Correlations of F_{HONO}_max and fertilization rates. The six F_{HONO}_max were obtained in summers of 2015 (fertilization rates: 0 and 45 kg-N ha^{-1}), 2016 (0, 350 and 247 kg-N ha^{-1}), and 2017 (180 kg-N ha^{-1}).

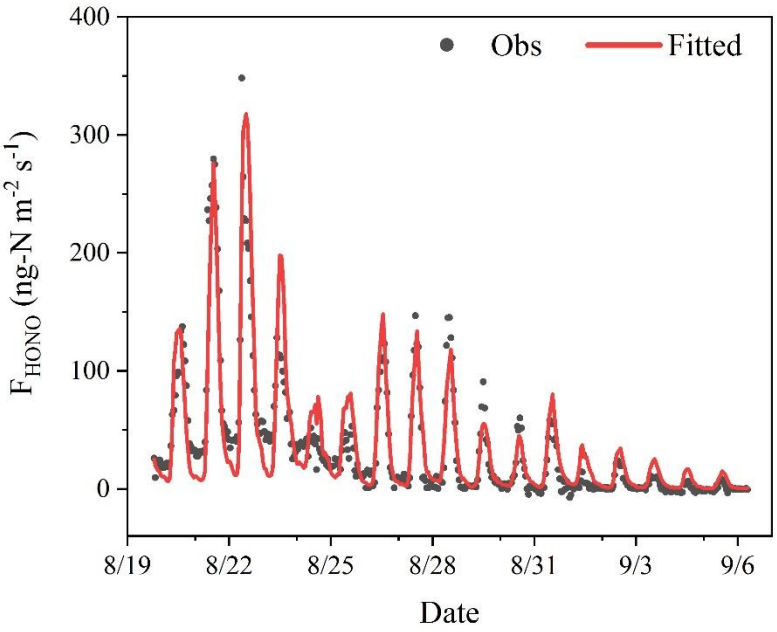

Figure S7: Comparison of HONO emission fluxes (F_{HONO}) observed from the fertilized field (Obs, black dot) and predicted by Equation R2 in the main text (Fitted, red line).

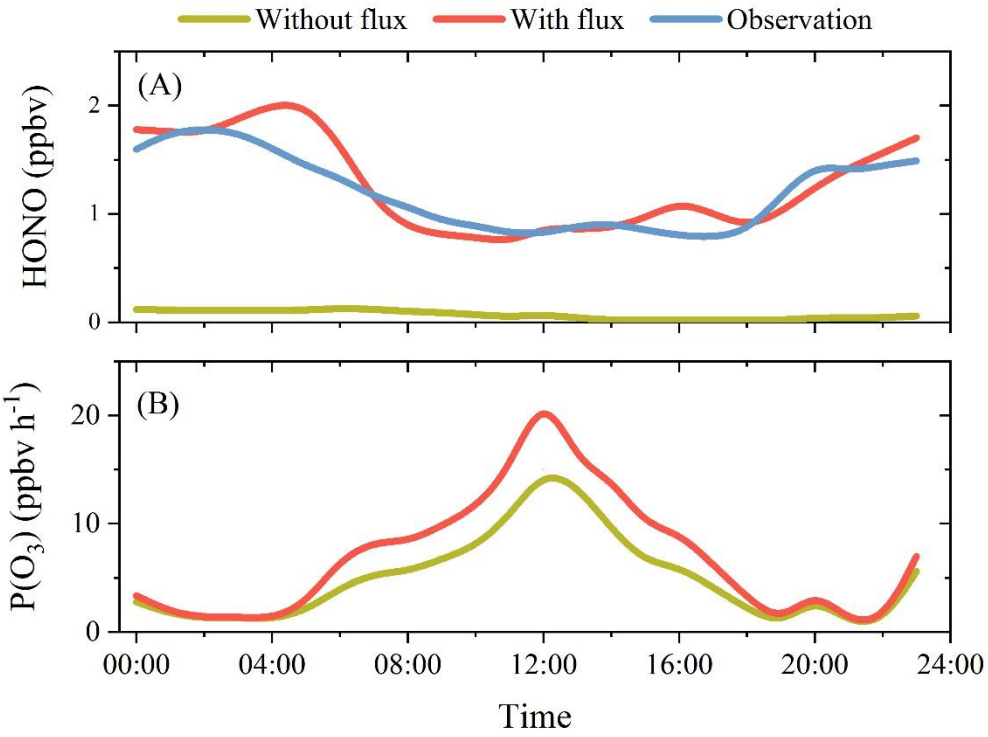

Figure S8: Results of box model simulations with/without HONO emission flux on (A) HONO and (B) O_3 production rate ($P(O_3)$).

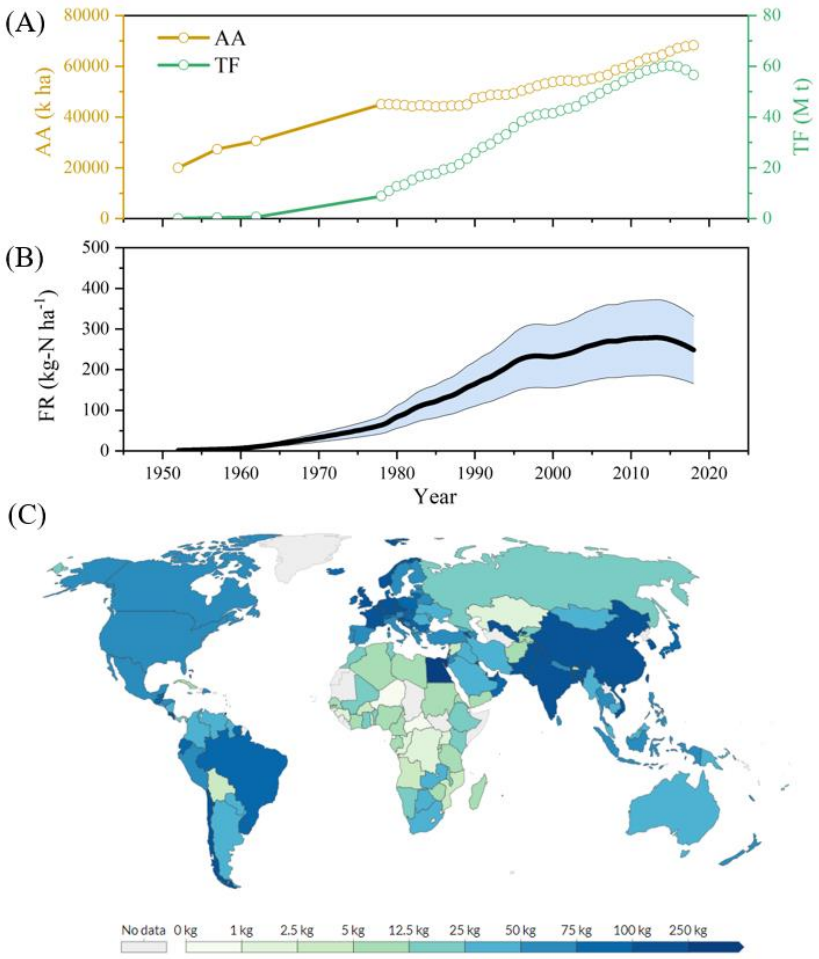

Figure S9: (A): Agricultural area (AA) and the total fertilizer application amount (TF) in China (Data source: China Rural Statistical Yearbook 2019); (B): Fertilizer application rates (FR) in China; (C): A summary of worldwide nitrogen fertilizer use per hectare of cropland in 2019 (Source: Our World in Data and UN Food and Agricultural Organization (FAO)).

6 References

(1) Zhang, J.; Xue, C.; Wang, D.; Qu, Y.; Chen, Y.; Mu, Y.; Guo, Y.; Wang, J.; An, J. Strong Photochemical Reactions in Greenhouses after Fertilization and Their Implications. *Atmos. Environ.* **2019**, *214*, 116821. https://doi.org/10.1016/j.atmosenv.2019.116821.

(2) Laufs, S.; Cazaunau, M.; Stella, P.; Kurtenbach, R.; Cellier, P.; Mellouki, A.; Loubet, B.; Kleffmann, J. Diurnal Fluxes of HONO above a Crop Rotation. *Atmos. Chem. Phys.* **2017**, *17* (11), 1–28. https://doi.org/10.5194/acp-17-6907-2017.

(3) von der Heyden, L.; Wißdorf, W.; Kurtenbach, R.; Kleffmann, J. A Relaxed Eddy Accumulation (REA) LOPAP-System for Flux Measurements of Nitrous Acid (HONO). *Atmos. Meas. Tech. Discuss.* **2021**, *2021*, 1–23. https://doi.org/10.5194/amt-2021-408.

(4) Xue, C.; Ye, C.; Zhang, Y.; Ma, Z.; Liu, P.; Zhang, C.; Zhao, X.; Liu, J.; Mu, Y. Development and Application of a Twin Open-Top Chambers Method to Measure Soil HONO Emission in the North China Plain. *Sci. Total Environ.* **2019**, *659*, 621–631. https://doi.org/10.1016/j.scitotenv.2018.12.245.

(5) Xue, C.; Zhang, C.; Ye, C.; Liu, P.; Catoire, V.; Krysztofiak, G.; Chen, H.; Ren, Y.; Zhao, X.; Wang, J.; Zhang, F.; Zhang, C.; Zhang, J.; An, J.; Wang, T.; Chen, J.; Kleffmann, J.; Mellouki, A.; Mu, Y. HONO Budget and Its Role in Nitrate Formation in the Rural North China Plain. *Environ. Sci. Technol.* **2020**, *54* (18), 11048–11057. https://doi.org/10.1021/acs.est.0c01832.

(6) Liu, Y.; Lu, K.; Li, X.; Dong, H.; Tan, Z.; Wang, H.; Zou, Q.; Wu, Y.; Zeng, L.; Hu, M.; Min, K.-E.; Kecorius, S.; Wiedensohler, A.; Zhang, Y. A Comprehensive Model Test of the HONO Sources Constrained to Field Measurements at Rural North China Plain. *Environ. Sci. Technol.* **2019**, *53* (7), 3517–3525. https://doi.org/10.1021/acs.est.8b06367.

(7) Xue, L. K.; Wang, T.; Gao, J.; Ding, A. J.; Zhou, X. H.; Blake, D. R.; Wang, X. F.; Saunders, S. M.; Fan, S. J.; Zuo, H. C.; Zhang, Q. Z.; Wang, W. X. Ground-Level Ozone in Four Chinese Cities: Precursors, Regional Transport and Heterogeneous Processes. *Atmos. Chem. Phys.* **2014**, *14* (23), 13175–13188. https://doi.org/10.5194/acp-14-13175-2014.

(8) Zhang, J.; An, J.; Qu, Y.; Liu, X.; Chen, Y. Impacts of Potential HONO Sources on the Concentrations of Oxidants and Secondary Organic Aerosols in the Beijing-Tianjin-Hebei Region of China. *Sci. Total Environ.* **2019**, *647*, 836–852. https://doi.org/10.1016/j.scitotenv.2018.08.030.

(9) Fu, X.; Wang, T.; Gao, J.; Wang, P.; Liu, Y.; Wang, S.; Zhao, B.; Xue, L. Persistent Heavy Winter Nitrate Pollution Driven by Increased Photochemical Oxidants in Northern China. *Environ. Sci. Technol.* **2020**, *54* (7), 3881–3889. https://doi.org/10.1021/acs.est.9b07248.

(10) Xing, L.; Wu, J.; Elser, M.; Tong, S.; Liu, S.; Li, X.; Liu, L.; Cao, J.; Zhou, J.; El-Haddad, I.; Huang, R.; Ge, M.; Tie, X.; Prévôt, A. S. H.; Li, G. Wintertime Secondary Organic Aerosol Formation in Beijing-Tianjin-Hebei (BTH): Contributions of HONO Sources and Heterogeneous Reactions. *Atmos. Chem. Phys.* **2019**, *19* (4), 2343–2359. https://doi.org/10.5194/acp-19-2343-2019.

(11) Sarwar, G.; Roselle, S. J.; Mathur, R.; Appel, W.; Dennis, R. L.; Vogel, B. A Comparison of CMAQ HONO Predictions with Observations from the Northeast Oxidant and Particle Study. *Atmos. Environ.* **2008**, *42* (23), 5760–5770. https://doi.org/10.1016/j.atmosenv.2007.12.065.

(12) Li, G.; Lei, W.; Zavala, M.; Volkamer, R.; Dusanter, S.; Stevens, P.; Molina, L. T. Impacts of

HONO Sources on the Photochemistry in Mexico City during the MCMA-2006/MILAGO Campaign. *Atmos. Chem. Phys.* **2010**, *10* (14), 6551–6567. https://doi.org/10.5194/acp-10-6551-2010.

(13) Zhang, L.; Wang, T.; Zhang, Q.; Zheng, J.; Xu, Z.; Lv, M. Potential Sources of Nitrous Acid (HONO) and Their Impacts on Ozone: A WRF-Chem Study in a Polluted Subtropical Region. *J. Geophys. Res. Atmos.* **2016**, *121* (7), 3645–3662. https://doi.org/10.1002/2015JD024468.

(14) Ha, P. T. M.; Kanaya, Y.; Taketani, F.; Dolores, M.; Hernández, A.; Pfeilsticker, K.; Sudo, K. Implementation of HONO into the Chemistry-Climate Model CHASER (V4 . 0): Roles in Tropospheric Chemistry. *Geosci. Model Dev. Discuss.* **2021**, No. 2, 1–44. https://doi.org/https://doi.org/10.5194/gmd-2021-385.

(15) Elshorbany, Y. F.; Steil, B.; Brühl, C.; Lelieveld, J. Impact of HONO on Global Atmospheric Chemistry Calculated with an Empirical Parameterization in the EMAC Model. *Atmos. Chem. Phys.* **2012**, *12* (20), 9977–10000. https://doi.org/10.5194/acp-12-9977-2012.

(16) Zhang, J.; Chen, J.; Xue, C.; Chen, H.; Zhang, Q.; Liu, X.; Mu, Y.; Guo, Y.; Wang, D.; Chen, Y.; Li, J.; Qu, Y.; An, J. Impacts of Six Potential HONO Sources on HO_x Budgets and SOA Formation during a Wintertime Heavy Haze Period in the North China Plain. *Sci. Total Environ.* **2019**, *681*, 110–123. https://doi.org/10.1016/j.scitotenv.2019.05.100.

(17) Goliff, W. S.; Stockwell, W. R.; Lawson, C. V. The Regional Atmospheric Chemistry Mechanism, Version 2. *Atmos. Environ.* **2013**, *68* (x), 174–185. https://doi.org/10.1016/j.atmosenv.2012.11.038.

(18) Xue, C.; Ye, C.; Zhang, C.; Catoire, V.; Liu, P.; Gu, R.; Zhang, J.; Ma, Z.; Zhao, X.; Zhang, W.; Ren, Y.; Krysztofiak, G.; Tong, S.; Xue, L.; An, J.; Ge, M.; Mellouki, A.; Mu, Y. Evidence for Strong HONO Emission from Fertilized Agricultural Fields and Its Remarkable Impact on Regional O_3 Pollution in the Summer North China Plain. *ACS Earth Sp. Chem.* **2021**, *5* (2), 340–347. https://doi.org/10.1021/acsearthspacechem.0c00314.